Modeling and Optimization of Piston Pumps for Drilling

Marius Stan
Mechanical Engineering Department, Petroleum-Gas University of Ploiesti, Romania
mstan@upg-ploiesti.ro

Dragos Gabriel Zisopol
Mechanical Engineering Department, Petroleum-Gas University of Ploiesti, Romania
zisopol@zisopol.ro
(corresponding author)

Received: 25 January 2023 | Revised: 20 February 2023 | Accepted: 28 February 2023

ABSTRACT

This study highlights the operational and practical advantages of using triplex mud pump systems in favor of duplex systems to optimize drilling capabilities under specific operational conditions. Additionally, the material selection of the piston subassembly was analyzed and simulated under operational parameters in SolidWorks to determine the advantages of using HNBR over NBR elastomer materials.

Keywords-pumps; piston; elastomer; finite element method; analysis

I. INTRODUCTION

Mud pumps ensure the flow required for the drilling rig process within the circulation system, as shown in Figure 1. Mud pumps are powerful machines that pull the drilling fluid from the tank, inject it through the drill rods to and from the foot of the well, and bring the fluid loaded with detritus resulting from the drilling process to the surface [1]. In optimal operating conditions, mud pumps consume more than 60% of the power used in the rotary drilling process. Two, to four mud pumps are normally used in drilling rigs, mainly in turn, while others are kept as spare parts in the event of a failure at the main working pump. Sometimes the pumps are tied together to lift large amounts of mud to the surface [1-4]. Modifications to the construction type of pump are required by the drilling process, such as types 3.1, 2.2, and 6.1. Pumps 3.1 and 6.1 are high-flow and medium-pressure, and 2.2 are high-pressure pumps with a smaller and more uniform flow. Mud pumps must be able to achieve a pressure of 1400 bar, within the individual power limit of 1830KW.

II. TECHNICAL AND THEORETICAL BASES OF MUD PUMP CALCULATION

Mud pumps generate hydraulic energy to achieve efficient and optimized drilling [1]. Research conducted in rock dislocation laboratories to develop a new drilling technology led to the practical conclusions shown in Table I.

A. Piston Size Calculation

The piston metal disc is calculated as a circular plate embedded in the cylindrical hub of diameter D_p=80mm, under pressure p_r=8.6347MPa, and a contour load given by the friction force between the piston and the cylinder, F_r=108N. The maximum unit efforts are calculated for circular with interior diameter constraint [1]:

$$\sigma_{rmax} = K_{r1}\frac{F_f}{h^2}_{t1}\frac{p_r \cdot r_2^2}{h^2} \quad (1)$$

$K_{r1} = -0.405$, $K_{t1} = -0.121$, $K_{r1}^p = -0.71$, and $K_{t1}^p = -0.213$.

where σ_{rmax} is the maximum radial tension, K_{r1} is the stiffness constant of the plate in the radial direction, F_f is the load force, h^2 is the thickness of the plate, K_{t1} is the stiffness constant of the plate in the axial direction, p_r is pressure, and r^2 is the radius. The area of maximum stress is the upper area of the hub. The unitary efforts are:

$$\sigma_1 = -\frac{2655}{h^2} \quad (2)$$

$$\sigma_2 = -\frac{1512}{h^2} \quad (3)$$

$$\sigma_3 = -86.347 \quad (4)$$

where σ_1, σ_2, and σ_3 are the main tensions, and thickness h is calculated according to the energy theory of rupture:

$$\sigma_{echiv} = \sqrt{\sigma_1^2 + \sigma_2^2 + \sigma_3^2 - (\sigma_1\sigma_2 + \sigma_2\sigma_3 + \sigma_3\sigma_1)} \leq \sigma_a \quad (5)$$

where σ_{echiv} is the equivalent stress in the stress resistance theory. The piston is made of E355 steel, which is a high-strength and low-alloy steel, good for manufacturing. It is allowed $\sigma_a = 120\text{N/mm}^2$. Equation (2) admitted h=20mm to calculate the sizing of the lantern lid. The cover of the lantern is required by a uniformly distributed pressure corresponding to

the test pressure. The lid can be assimilated with a double-recessed circular plate p_b=19.4MPa and R=100mm.

TABLE I. WORKING PARAMETERS OF PUMPS

Column [in]	$16\frac{3}{4}$"	$13\frac{3}{8}$"	$9\frac{5}{8}$"	$6\frac{5}{8}$"
Q [dm^3/s]	104	69.60	34.20	16.50
p [MPa]	8.6347	12.8860	7.56512	12.91255

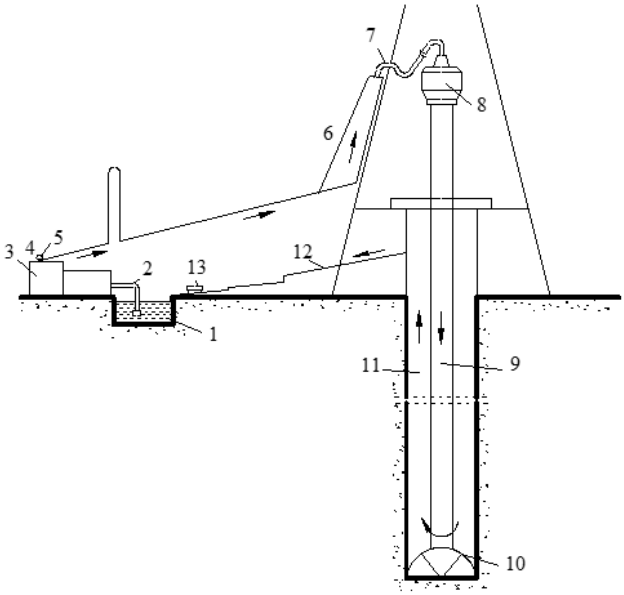

Fig. 1. Circulation system diagram: 1: battle, 2: suction pipe, 3: mud pump, 4: pushing pipe, 5: shock absorber, 6: charger, 7: hydraulic hose, 8: hydraulic head, 9: drilling rig, 10: screed holes, 11: annular space, 12: gutter system, 13: cleaning device.

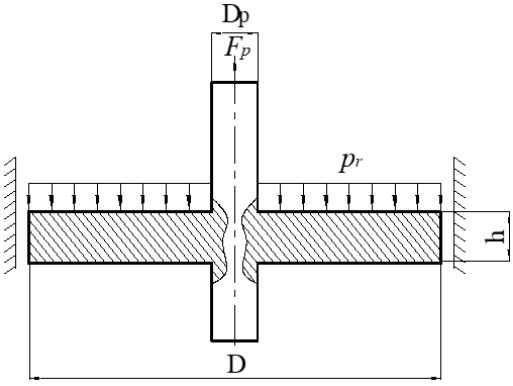

Fig. 2. Piston calculation scheme.

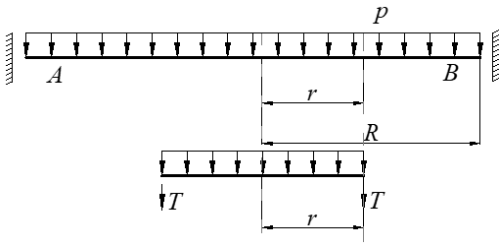

Fig. 3. Lantern cover calculation scheme.

$$T = -\frac{p_b \cdot r}{2}$$
$$\frac{d}{dr}\left[\frac{1}{r}\cdot\frac{d}{dr}\cdot(r\phi)\right] = -\frac{T}{D} \quad (6)$$
$$\frac{d}{dr}\left[\frac{1}{r}\cdot\frac{d}{dr}\cdot(r\phi)\right] = -\frac{p_b \cdot r}{2 \cdot D}$$

where T is the cut force, p_b is the pressure on the gross surface of the piston, r is the radius, d is the rod diameter, and D is the cylindrical bending stiffness of the plate [1]:

$$M_\theta = -\mu \cdot D \cdot \frac{d\phi}{dr}$$
$$\Rightarrow M_\theta = -\mu \cdot D \cdot \frac{p_b}{16 \cdot D}\cdot(R^2 - 3\cdot r^2) \quad (7)$$
$$M_r = -D \cdot \frac{d\phi}{dr} \Rightarrow M_\theta = -D \cdot \frac{p_b}{16 \cdot D}\cdot(R^2 - 3\cdot r^2)$$

where M_θ, M_r is the bending moment in the tangential or radial direction of the circular plate. Table II shows the results for r=R.

TABLE II. RESULTS FOR $r = R$

Efforts in plate	M_θ	M_r
Values[kN]	-8.08	-24.25
Unitar Tensions in plate	σ_θ	σ_r
Values relations calculus for thickness h [kPa]	14.550/h^2	4.848/h^2

The resistance condition is given by:

$$\sigma_r \cdot \sigma_\theta > 0\ ;\ |\sigma_r| \le \sigma_a\ ;\ |\sigma_\theta| \le \sigma_a \quad (8)$$

The lantern cover is made of E355, AISI/SAE/ASTM 1024, with σ_a=180N/mm^2 and h=35mm. Double-acting mud pumps have two-sided active pistons, and single-acting pistons use either plunger-type pistons or single-sided active pistons. A single-sided active piston has only one construction seal that is structurally similar to that of a two-sided active piston and removable seals. This lining is met on the back with a thick cloth insert that stops discharge. The piston rod connects the piston and the crosshead. At both ends of the piston, the rod ends with a conical and a cylindrical threaded part that connects to the piston body and the cross-head or with the extending rod [5-6]. The rod and the piston have parts such as the connecting thread, the conical head of the rod, and the interchangeable piston hole, as regulated by the API 7K norms.

B. Determination of the Efforts in the Piston Rod

Figure 4 shows the forces acting on the piston rod.

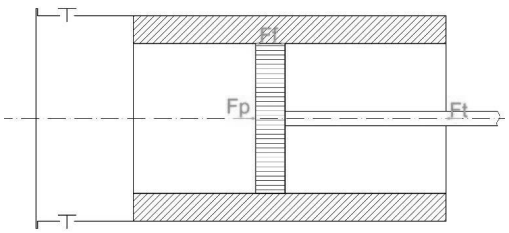

Fig. 4. Piston rod loading scheme.

$$F_t = F_p + F_f \quad (9)$$

where F_t is the total force acting on the piston rod for the single-acting triplex pump, F_p is the force due to pressure on the active face of the piston, and F_f is the friction force that appears between the jacket and the piston.

$$F_p = \frac{\pi \cdot D^2}{4} \cdot p \quad (10)$$

where p is the pressure acting on the piston face.

$$F_f = \mu \cdot N \cdot D \cdot l1 \quad (11)$$

where μ is the coefficient of friction, $\mu = 0.02 \ldots 0.1$, N is the normal reaction of the cylinder-piston interaction, D is the piston diameter, and $l1$ is the length of the sealing element.

C. Calculation of Piston Thickness

The thickness of the piston metal disc is calculated by considering the disc as a circular plate embedded in the cylindrical hub of diameter d_b subjected to pressure. Figure 5 shows the piston loading diagram. This problem can be solved by considering the symmetrically charged flat plates, as in Figure 6.

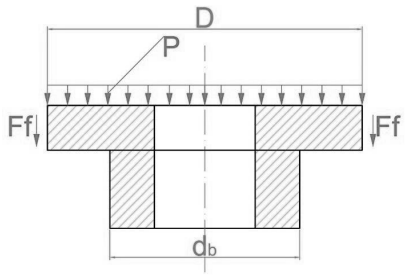

Fig. 5. Piston rod loading pattern.

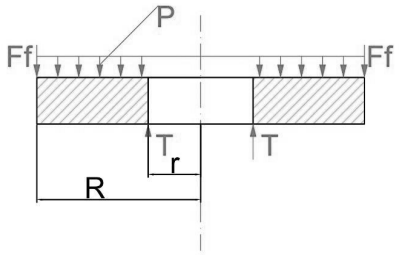

Fig. 6. Charging scheme corresponding to symmetrically charged plates.

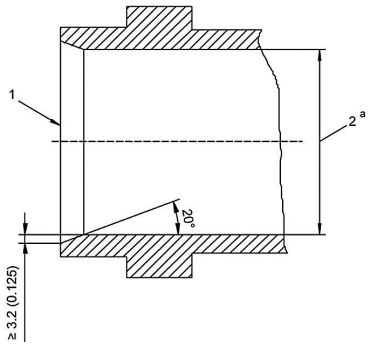

Fig. 7. Piston-cylinder concentricity for mud pumps: 1: the insertion end of the piston, 2: piston lining; a - nominal diameter tolerance.

III. MODELING AND SIMULATION

A. The 7K API Recommendations for Design Basics

According to the API 7K standard, mud pumps are piston pumps that have certain construction bases. The most important considered for this study are:

- The main load-bearing components perform the pump discharge pressure, except for consumables and shut-off components such as gaskets, pistons, piston rods, seals, valves and seats, caps, clamps, bushings, and fasteners.
- Pressure-evaluated components must be subjected to a test pressure 3.5 times higher than the operational working pressure. Hydraulic testing is performed according to API Chapter 8.7.
- The design of the suction components of the mud pump of the hydrostatic circuit must take into account that the suction pressure during the test will have a value twice higher than the one required by the applicant.
- For double-acting pumps, the fluid outlets from the mud pump cylinders and from the piston body.
- Mud pump pistons must match the standard concentricity of the piston rod. The outer diameters of the piston must be suitable for the use of gaskets or cylinders with increases or changes in diameter.

The standardized dimensions of the main components of mud pumps are presented in the appendices of the API 7K standard. For example, Annex C provides recommendations for the mud pump piston, terminology, and maintenance, while the provisions regarding the outlet area of the drilling fluid in Annex C.3 are very important. The recommendations for mud pump piston standardize the terminology for the main parts of the mud pump, except for a relatively small number of related parts. This provides a common language for the industry, which is especially important for communication.

B. 3D Modeling of the Piston

Mud pump piston modeling is performed using 3D graphic modeling and a finite element calculation program. This piston was made of low alloy medium carbon steel 34CrMo4 in SR EN 10083-3 and made of an NBR elastomer with an elastic modulus of 3.99MPa [7-9]. According to [10], the material yield strength is σ_c=450MPa. The pump piston was machined in steps and its diameter varied in different sections [8]. The piston assembly had 190.5mm outer diameter and 100mm thickness. The function 'sketch' was used to model the metal part of the piston and choose the drawing plan, as seen in Figure 9. After that, a circle was drawn on the front plane, which would be extruded to obtain a cylindrical body to represent one of the steps of the drive piston. The 2D sketch of the lower diameter was made, after which the extrusion was to create the 3D shape of the metal part of the piston, as seen in Figure 10. Then, the piston elastomer was made using the same steps. Instead of the 'Extrude' function, the 'Cut Extrude' was used to get the desired shape for the metal piston, as seen in Figure 11. Finally, an assembly was made that consisted of the metal part of the piston and the elastomer.

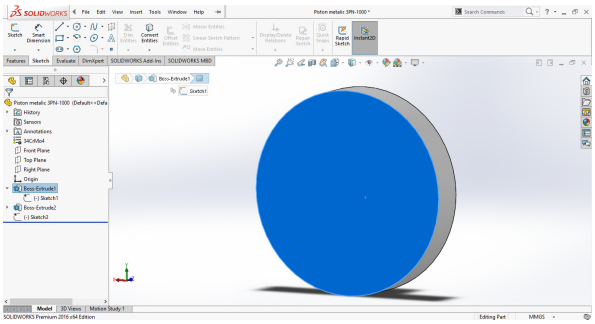

Fig. 8. Drawing plane of the piston.

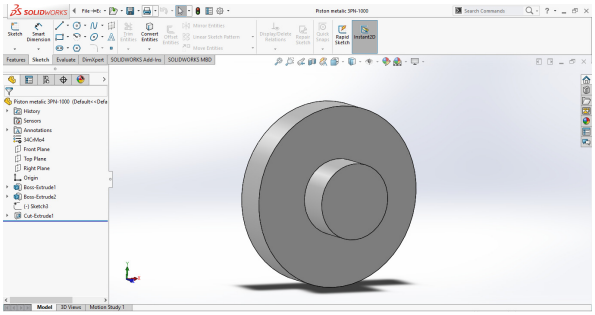

Fig. 9. Metalic part of the piston.

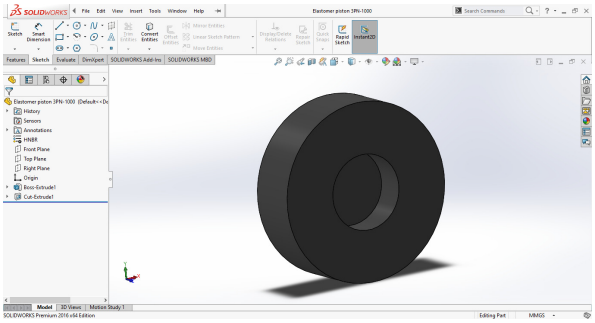

Fig. 10. Piston elastomer.

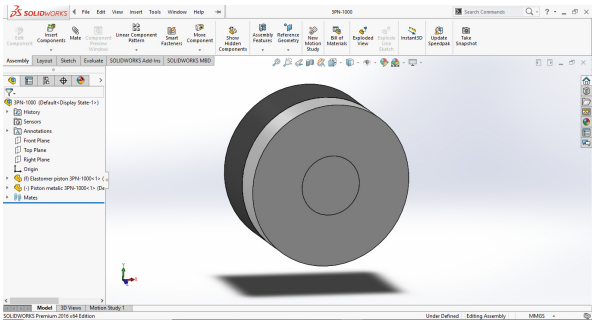

Fig. 11. Complete assembly of the piston.

C. Finite Element Analysis of 3PN-1000 Pump Piston Strain Study to Rated Operating Pressure

A simulation was performed to complete the study. The piston components were: the metal piston had a material of 34CrMo4 and the elastomer was Nitrile Butadiene Rubber (NBR) [8, 12]. A full 3D model was chosen for the finite element analysis [13]. A fixed face was established, that defined the metal part of the piston as fixed. This action can be done from the study toolbar by right-clicking on "Fixture", then choosing the "Fixed geometry" module [14].

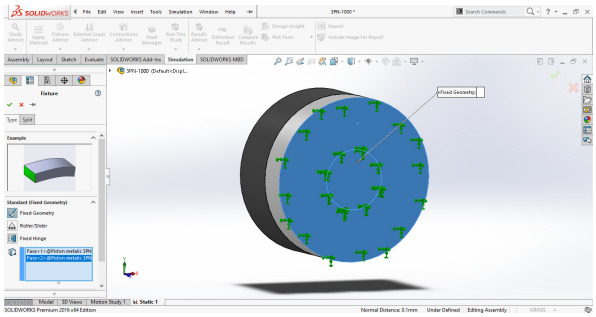

Fig. 12. Defining the fixed face of the piston.

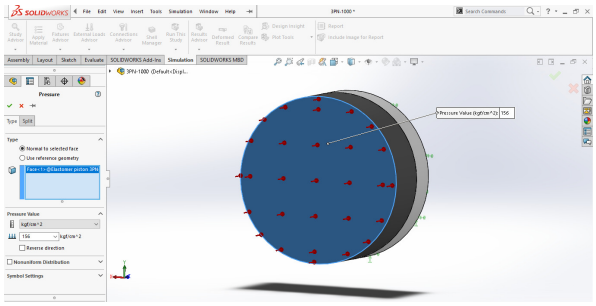

Fig. 13. Pressure applied to piston elastomer (rear).

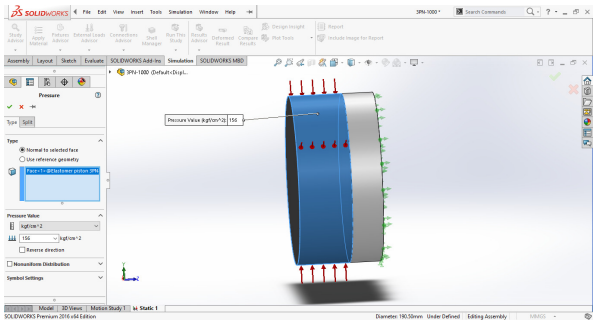

Fig. 14. Pressure applied to the piston elastomer (outside).

The next step was to define the nominal pressure to which the piston would be subjected, namely the pressure between the elastomer and the top cover of the piston jacket. The nominal pressure was set to 156MPa. The same procedure was applied to the upper part of the elastomer for the pressure between the piston sleeve and the elastomer. Then a simulation was performed to examine how the piston deforms under the assigned loads. As can be seen in Figures 15-18, the deformation of the piston was free, that is, the piston deformed in an open space but not inside the cylinder. Due to this deformation, there is a possibility of fluid leakage between the piston sleeve and the piston. Table III presents the principal properties of the NBR material for the first simulation [2, 5, 9]. The dimensions for the finite element analysis were D=133/5mm, d=80mm, and h=40mm, which impact the results obtained from the analysis. The area that suffers the most

deformation is marked in red. The images show the initial position of the piston elastomer and how it deformed.

TABLE III. MATERIAL OF THE NBR ELASTOMER [11]

Property	Value	Units
Elastic modulus	3990000	N/m^2
Poisson ratio	0.49	N/A
Shear modulus	2900000	N/m^2
Mass density	1000	kg/m^3
Tensile strength	13787100	N/m^2
Compressive strength		N/m^2
Yield strength	9237370	N/m^2
Thermal expansion coefficient	0.00067	/K
Thermal conductivity	0.14	W/(m•K)

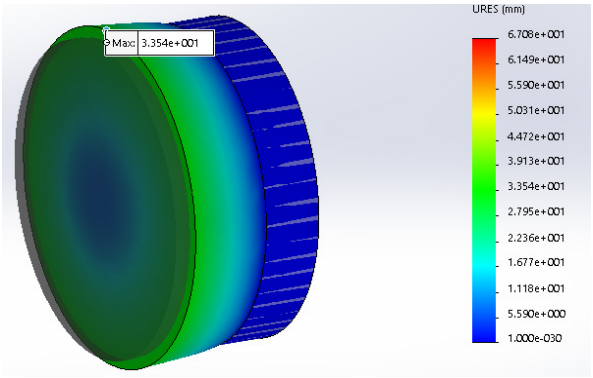

Fig. 15. Deformation of the NBR piston at ½ from the nominal pressure.

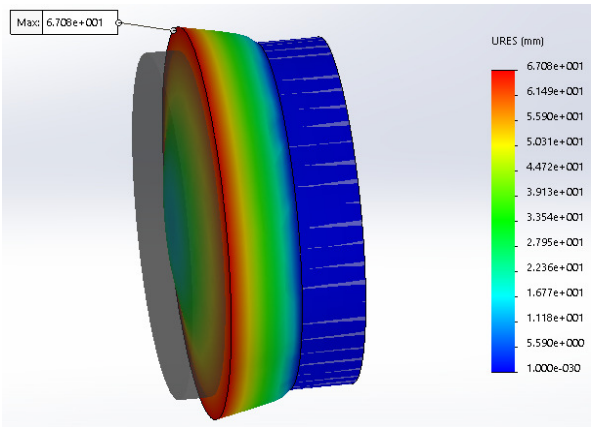

Fig. 16. Deformation of the piston with NBR at nominal pressure.

TABLE IV. MATERIAL OF THE HNBR ELASTOMER

Property	Value	Units
Elastic modulus	3430000	N/m^2
Poisson ratio	0.49	N/A
Shear modulus	2900000	N/m^2
Mass density	1200	kg/m^3
Tensile strength	20787100	N/m^2
Compressive strength		N/m^2
Yield strength	9237370	N/m^2
Thermal expansion coefficient	0.00067	/K
Thermal conductivity	0.14	W/(m•K)

In terms of stress, a "strain" graph can be used to determine the most requested point of the piston when operating at a pressure of 15.6MPa. Table V shows the deformation details of the piston with the NBR and HNBR materials.

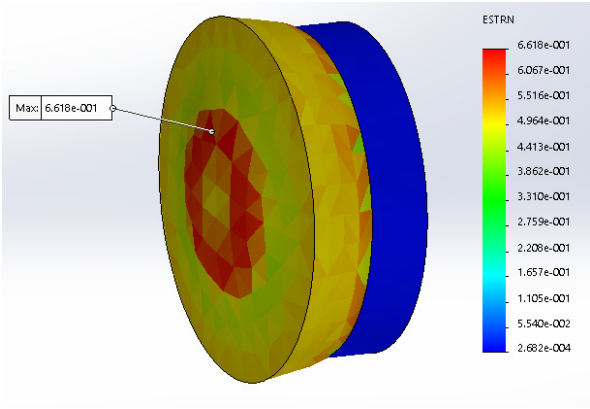

Fig. 17. Equivalent strains of HNBR elastomer.

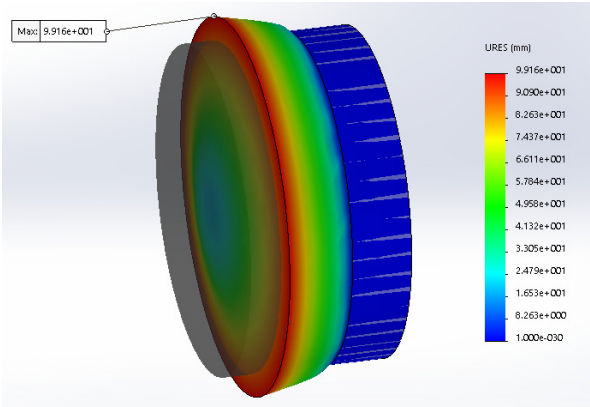

Fig. 18. Deformation of the piston with HNBR.

TABLE V. RESULTS OBTAINED FROM THE PROCESSING OF FEA DIAGRAMS

No.	Type parameter FEA	Pressure in pump (MPa)	NBR (mm)	HNBR (mm)
1	Equivalent strain (ESTRN)	35	2.84	1.94
		15.6	2.499	1.447
2	Resultant displacement (URES)	15.6	6.708	9.016
		7.8	3.354	4.508

IV. CONCLUSIONS

This study investigated new types of rubber-to-gasket piston connections, namely NBR and HNBR. The mechanical performance of both was systematically studied using theoretical and finite element analysis methods. Compared to the traditional criteria, the following conclusions were obtained:

- Simulations of NBR and HNBR piston elastomer materials [9] showed that in a mud pump with large diameter pistons operating at low pressures, the NBR can be used as it deforms sufficiently so that fluid losses are not high and the friction between the jacket and the piston is optimal.
- In the case of mud pumps with small diameter pistons and high pressures, the HNBR elastomer can be used because it

deforms much more easily than the NBR, the liquid losses will be lower, but instead, there would be more friction between the piston and the cylinder, but in no case excessive.

- The operating season of the mud pump can be taken into account. For example, in winter, the HNBR can deform much more easily at low temperatures compared to NBR, while in summer both can be used. The stresses on the HNBR elastomer are distributed differently than those on the NBR. In the case of the HNBR elastomer, there are no longer stresses on the contact surface between the elastomer and the metal piston.
- The SolidWorks software can perform finite element analysis studies of both parts and assemblies to validate rig performance. This capacity enables the custom rig manufacturer to improve the strength and performance of its equipment while decreasing weight, material usage, and associated costs in the process.
- The material and weight of the rigs should be reduced because they are frequently assembled on the back of a truck. Using professional software, linear static stress analyses can run not only on critical components but also on each sub-assembly of the piston pump. This capability allows for reducing the weight of the rigs by a small percentage while maintaining strength and performance.

REFERENCES

[1] M. Stan, *Metode avansate de proiectare a utilajului petrolier*. Ploiesti, Romania: Editura Universităţii Petrol-Gaze din Ploiesti, 2010.

[2] D. G. Zisopol, M. Minescu, M. Badicioiu, and M. M. Caltaru, "Theoretical and Experimental Investigations on 20 Inches Threaded Casing Connections Failure under Field Conditions," *Engineering, Technology & Applied Science Research*, vol. 11, no. 4, pp. 7464–7468, Aug. 2021, https://doi.org/10.48084/etasr.4318.

[3] M. Elashmawy, "3D-CFD Simulation of Confined Cross-Flow Injection Process Using Single Piston Pump," *Engineering, Technology & Applied Science Research*, vol. 7, no. 6, pp. 2308–2312, Dec. 2017, https://doi.org/10.48084/etasr.1561.

[4] D. G. Zisopol, "Experimental research concerning drill pipe geometry optimization," *Lucrarile Sesiunii de Comunicari Stiintifice*, vol. 4, pp. 169–178, Jan. 1997.

[5] D. G. Zisopol, "Experimental research related to the behaviour of the materials afferent to the liners and the pistons for production pumps under wear conditions," 2004, [Online]. Available: https://essuir.sumdu.edu.ua/handle/123456789/10739.

[6] M. M. Caltaru, R. G. Ripeanu, M. Badicioiu, and D. G. Zisopol, "Experimental Researches to Establish the Optimum Hardbanding Technology and Materials of the Heavy Weight Drill Pipe," *MATEC Web of Conferences*, vol. 318, 2020, Art. No. 01017, https://doi.org/10.1051/matecconf/202031801017.

[7] D. G. Zisopol and A. Dumitrescu, *Ecotehnologie. Studii de caz*. Ploiesti, Romania: Editura Universităţii Petrol-Gaze din Ploiesti, 2020.

[8] D. G. Zisopol and A. Dumitrescu, *Materiale si Tehnologii Primare. Aplicaţii practice şi studii de caz.* Ploiesti, Romania: Editura Universitatii din Ploiesti, 2005.

[9] M. Minescu and D. Zisopol, *Sudarea ţevilor şi fitingurilor din polietilenă de înaltă densitate*. Ploiesti, Romania: Editura Universităţii Petrol-Gaze din Ploiesti, 2021.

[10] D. G. Zisopol, M. Minescu, and D. V. Iacob, "A Theoretical-Experimental Study on the Influence of FDM Parameters on the Dimensions of Cylindrical Spur Gears Made of PLA," *Engineering, Technology & Applied Science Research*, vol. 13, no. 2, pp. 10471–10477, Apr. 2023, https://doi.org/10.48084/etasr.5733.

[11] "Solidworks 3D CAD Design Software." Dassault Systemes, [Online]. Available: https://www.solidworks.com/.

[12] M. M. Caltaru, M. Badicioiu, A. Dinita, D. G. Zisopol, R. G. Ripeanu, and M. Minescu, "Influence of Chemical Corrosive Environment with H2S on Drill Strings, Experimental Researches," *Revista de Chimie*, vol. 71, no. 4, pp. 29–37, May 2020, https://doi.org/10.37358/RC.20.4.8040.

[13] I. Lambrescu and D. G. Zisopol, "Complex analysis of collapse strength for tubulars used in the oil and gas industry," *Geoenergy Science and Engineering*, vol. 221, Feb. 2023, Art. no. 111275, https://doi.org/10.1016/j.petrol.2022.111275.

[14] D. G. Zisopol, D. V. Iacob, and A. I. Portoaca, "A Theoretical-Experimental Study of the Influence of FDM Parameters on PLA Spur Gear Stiffness," *Engineering, Technology & Applied Science Research*, vol. 12, no. 5, pp. 9329–9335, Oct. 2022, https://doi.org/10.48084/etasr.5183.